by M. Ragulskis, L. Saunoriene, and R. Maskeliunas

THE STRUCTURE OF MOIRÉ GRATING LINES AND ITS INFLUENCE TO TIME-AVERAGED FRINGES

Geometric moiré [1,2] is a classical in-plane whole-field non-destructive optical experimental technique based on analysis of visual patterns produced by superposition of two regular gratings that geometrically interfere. Examples of gratings are equispaced parallel lines, concentric circles, and arrays of dots.[2,3] The gratings can be superposed by double-exposure photography, by reflection, by shadowing, or by direct contact.[4,5] Moiré patterns are used to measure variables such as displacements, rotations, curvature, and strain throughout the viewed area. In-plane moiré is typically conducted with gratings of equispaced, parallel lines.[2,4]

A moiré grating on the surface of a one-dimensional structure in the state of equilibrium can be interpreted as a periodic variation of black and white colors. Continuous harmonic moiré functions are well applicable for digital image processing in computational environments[2]:

$$F(x) = \frac{1}{2} + \frac{1}{2}\cos\left(\frac{2\pi}{\lambda}x\right), \tag{1}$$

where x is the longitudinal coordinate, λ is the pitch of the grating, $F(x)$ is the grayscale level, numerical value 0 corresponds to black color, and 1 corresponds to white color.

Double-exposure geometric moiré techniques can be extended to time-average geometric moiré methods when the moiré grating is formed on the surface of elastic oscillating structures, and time-averaging techniques are used for registration of time-averaged patterns of fringes.[6,7] Let us assume that the deflections from the state of equilibrium oscillate in time. If time-averaging techniques are used to register the image of the oscillating structure, and the exposure time is much longer than the period of oscillation, the resulting pattern is formed as an integral sum of the continuous process of motion:

$$\begin{aligned} H_A F(x) &= \frac{1}{2} + \frac{1}{2}\lim_{T\to\infty}\frac{1}{T}\int_0^T \cos\left(\frac{2\pi}{\lambda}(x - A\sin(\omega t + \varphi))\right)\mathrm{d}t \\ &= \frac{1}{2} + \frac{1}{2}\cos\left(\frac{2\pi}{\lambda}x\right)J_0\left(\frac{2\pi}{\lambda}A\right), \end{aligned} \tag{2}$$

where $H_A F(x)$ is the operator of time averaging of a grayscale function,[8] T is the exposure time, A is the amplitude of oscillations, ω is angular velocity, φ is phase, J_0 is the zero-order Bessel function of the first kind. The explicit relationship among the fringe order, pitch of the grating, and dynamic displacement is obtained from the condition requiring that the value of the Bessel function is equal to 0 at the center of the time-averaged fringe:

$$A = \frac{\lambda}{2\pi}r_n, \tag{3}$$

where r_n is the nth root of the zero-order Bessel function of the first kind.

The result in Eq. 3 is clear and simple; it enables straightforward applicability of inverse engineering techniques for reconstruction of dynamic deflections from patterns of time-averaged fringes. Automatic, semiautomatic, or even manual fringe-counting techniques can be used for numerating fringes and determining the orders of Bessel function's roots in Eq. 3.

The result in Eq. 3 is based on the assumption that the variation of grayscale in the moiré grating (in the state of equilibrium) is governed by a harmonic function (Eq. 1). But whenever a geometric moiré grating is considered in a practical application, one usually has in mind an array of dark and bright bands on the surface of the analyzed structure. How would the relationship among the fringe order, pitch of the grating, and dynamic displacement change then?

Moreover, printing of dark bands on a bright deformable surface (or bright bands on a dark surface) is not always a simple technical task. What would happen if the width of the dark bands is not equal to 0.5 of the pitch of the grating? How can the time-averaged fringes be interpreted if, for example, the width of the dark bands is equal to one-third of the pitch?

The objective of this article is to give answers to the aforementioned questions and provide insight into the formation of time-averaged fringes generated by more complex moiré gratings.

ANALYTICAL RELATIONSHIPS

Suppose that a periodic one-dimensional grayscale function $F(x)$ with a period $2l$ can be expanded into a Fourier series:

$$F(x) = \frac{a_0}{2} + \sum_{n=1}^{+\infty}\left(a_n\cos\frac{n\pi x}{l} + b_n\sin\frac{n\pi x}{l}\right), \tag{4}$$

where a_0, a_n, and b_n are Fourier expansion coefficients (real numbers). Let us assume that $F(x)$ defines grayscale level on a surface of a one-dimensional structure and that structure oscillates in time. Then, time-averaged grayscale image of

M. Ragulskis (SEM member; minvydas.ragulskis@ktu.edu) is a professor and L. Saunoriene is a lecturer and research associate in the Research Group for Mathematical and Numerical Analysis of Dynamical Systems, Department of Mathematical Research in Systems at the Kaunas University of Technology, Kaunas, Lithuania. R. Maskeliunas is a professor in the Department of Printing Machines at the Vilnius Gediminas Technical University, Vilnius, Lithuania

doi: 10.1111/j.1747-1567.2009.00376.x

this oscillating structure (when time of exposure tends to infinity) could be expressed in the following form[8,9]:

$$H_A F(x) = \frac{a_0}{2} + \sum_{n=1}^{+\infty} \left(a_n \cos \frac{n\pi x}{l} + b_n \sin \frac{n\pi x}{l} \right) J_0 \left(\frac{n\pi A}{l} \right), \quad (5)$$

where H_A is the time-averaging operator.[8]

The analytical relationship described by Eq. 5 enables explicit analysis of the formation of time-averaged fringes for a stepped grayscale function:

$$F(x) = \begin{cases} 1, x \in \left[\lambda k; \frac{(1-s)\lambda}{2} + \lambda k \right] \cup \left[\frac{(1+s)\lambda}{2} + \lambda k; \lambda(k+1) \right] \\ 0, x \in \left(\frac{(1-s)\lambda}{2} + \lambda k; \frac{(1+s)\lambda}{2} + \lambda k \right) \\ k = 0,1,2,\ldots \end{cases} \quad (6)$$

where parameter s determines the width of the dark band; $0 \leqslant s \leqslant 1$ (Fig. 1b). It must be noted that the dark band of the stepped function is located symmetrically around the centerline of the pitch even if the grating itself is asymmetric in the sense that the widths of dark and white bands are not equal.

Expansion of the stepped grayscale function in a Fourier series yields the following expressions of the coefficients in Eq. 4:

$$a_0 = 2(1-s);$$

$$a_n = \frac{\sin(n\pi(1-s)) - \sin(n\pi(1+s))}{n\pi}, \quad n = 1,2,3,\ldots;$$

$$b_n = \frac{\cos(n\pi(1+s)) - \cos(n\pi(1-s))}{n\pi}, \quad n = 1,2,3,\ldots, \quad (7)$$

Now, the time-averaged digital image can be expressed in the form of Eq. 5 at $2l = \lambda$. A computationally reconstructed pattern of fringes is shown in Fig. 2b. Though time-averaged fringes are clearly visible by a naked eye, it is quite hard to identify the exact location of the centerlines of those fringes. Therefore, we calculate standard deviation of the grayscale

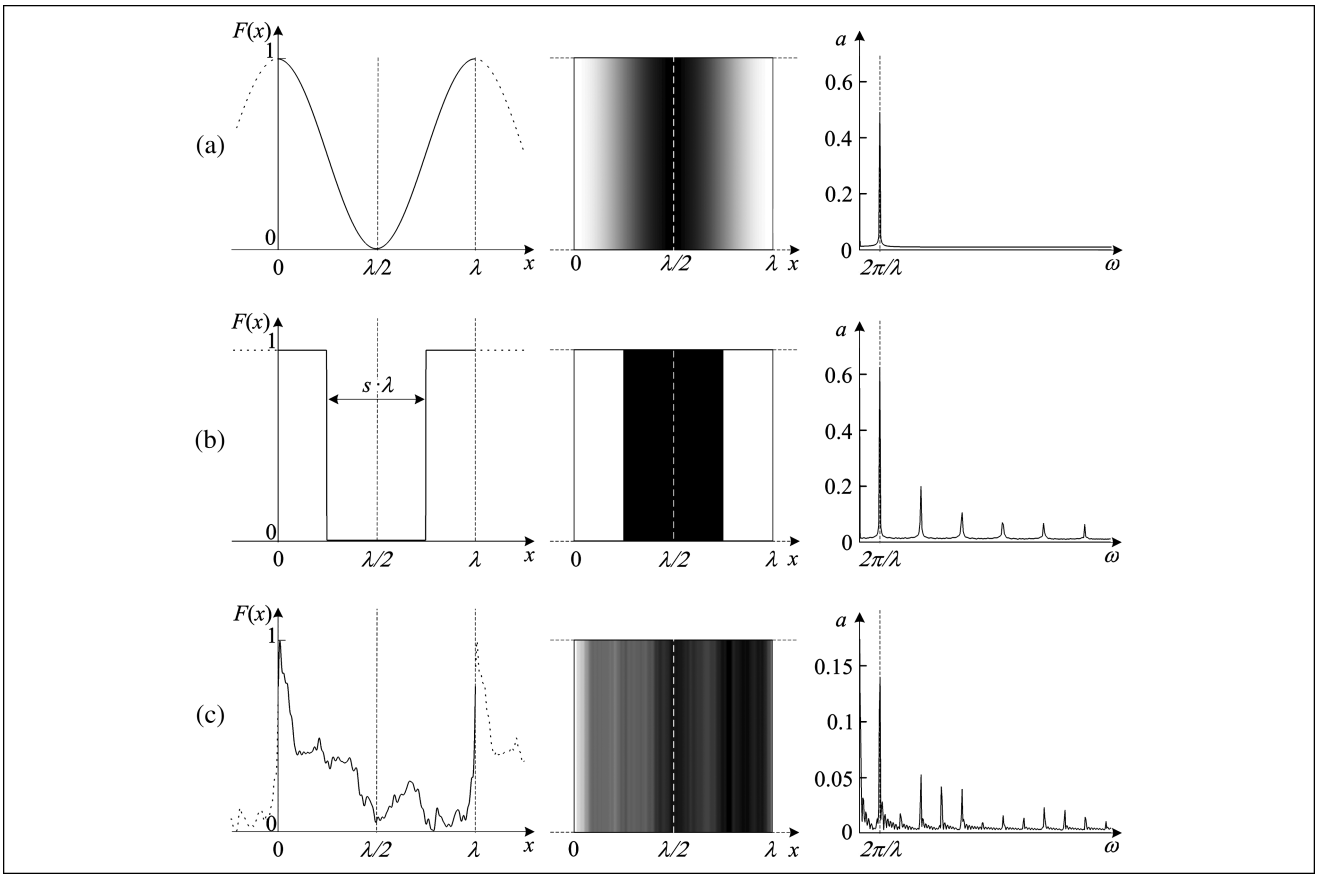

Fig. 1: Grayscale functions $F(x)$ (the first column), their representation in the grayscale color format (the second column), and Fourier amplitude spectrum (the third column) for (a) harmonic function, (b) stepped function, and (c) stochastic grayscale function

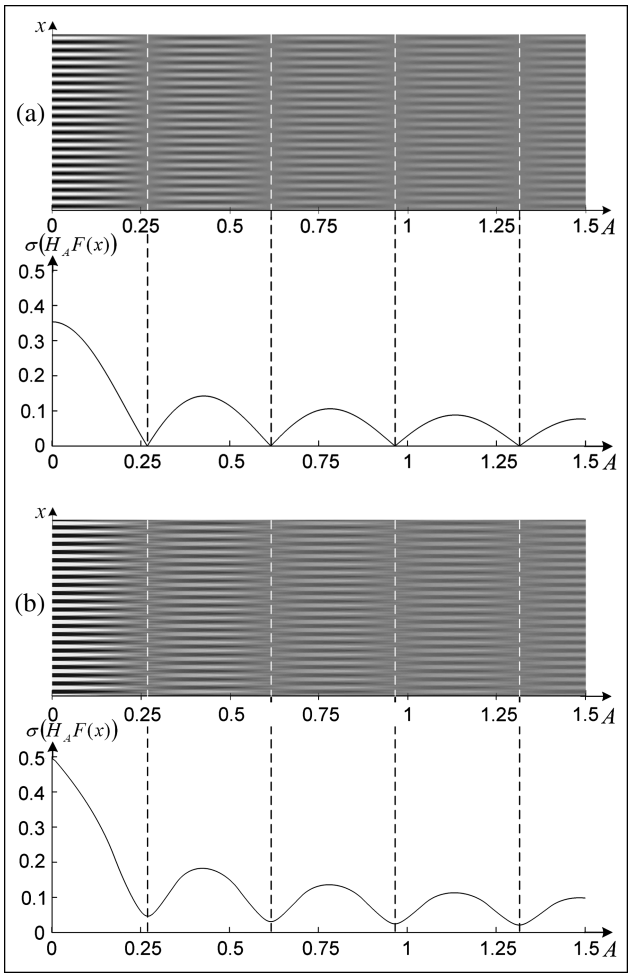

Fig. 2: Computationally reconstructed pattern of fringes for symmetric moiré gratings: (a) harmonic grating, $\lambda = 0.7$ and (b) stepped grating, $s = 0.5$, $\lambda = 0.7$

level around 0.5 at fixed A. It can be noted that these calculations are straightforward for harmonic moiré grating:

$$\sigma^2(H_A F(x)) = \frac{1}{\lambda}\int_0^{\lambda} (H_A F(x) - E(H_A F(x)))^2 dx$$

$$= \frac{1}{\lambda}\int_0^{\lambda} \left(\frac{1}{2} + \frac{1}{2}\cos\left(\frac{2\pi}{\lambda}x\right) J_0\left(\frac{2\pi}{\lambda}A\right) - \frac{1}{2}\right)^2 \mathrm{d}x \qquad (8)$$

$$= \frac{1}{4\lambda} J_0^2\left(\frac{2\pi}{\lambda}A\right) \cdot \int_0^{\lambda} \cos^2\left(\frac{2\pi}{\lambda}x\right) \mathrm{d}x = \frac{J_0\left(\frac{2\pi}{\lambda}A\right)^2}{8};$$

$$\sigma(H_A F(x)) = \frac{\left|J_0\left(\frac{2\pi}{\lambda}A\right)\right|}{\sqrt{8}}. \qquad (9)$$

Computationally reconstructed standard deviation $\sigma(H_A F(x))$ for harmonic moiré grating (Fig. 2a) shows sharp centerlines at such amplitudes A where $\frac{2\pi}{\lambda}A = r_n$ (Eq. 9). Standard deviation for stepped moiré grating at $s = 0.5$ also shows clear local minimums exactly at the same amplitudes as for harmonic moiré grating. The first important conclusion is that the pattern of centerlines of time-averaged fringes generated by harmonic and stepped symmetric moiré gratings coincide.

ASYMMETRIC GRATINGS

Next, we investigate the pattern of time-averaged fringes produced by asymmetric stepped moiré grating. First, we assume that $s = 0.8$. The pattern of time-averaged fringes and standard deviation are shown in Fig. 3a. Dashed lines correspond to centerlines of time-averaged fringes produced by harmonic grating and pointed dashed lines by asymmetric stepped moiré grating. A shift of the centerlines toward higher amplitudes can be observed in Fig. 3a. By the way, amplitude increments for fringes of different orders are practically identical.

Analogous simulations are performed for asymmetric stepped moiré grating at $s = 0.2$ (Fig. 3b). Again, a shift of the centerlines can be observed. Interesting is the fact that this shift also occurs toward higher amplitudes.

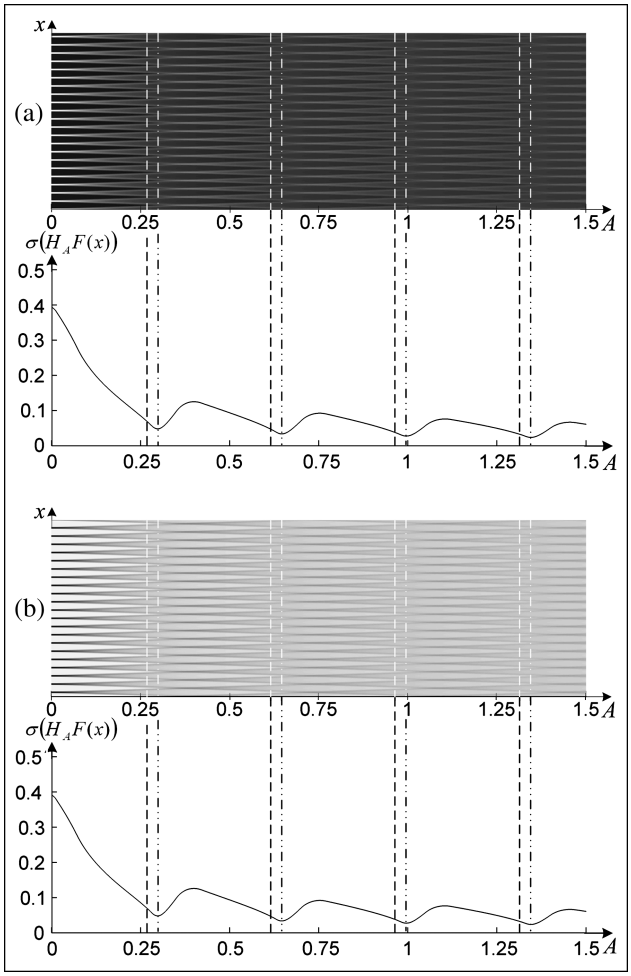

Fig. 3: Computationally reconstructed pattern of fringes for asymmetric stepped moiré grating: (a) $s = 0.8$, $\lambda = 0.7$ and (b) $s = 0.2$, $\lambda = 0.7$

Amplitude increments (shifts of the centerlines of time-averaged fringes) for different coefficients of asymmetry s and pitch λ are quantified in Fig. 4a. Nondimensional shifts of the centerlines of time-averaged fringes generated by stepped moiré gratings are presented in Fig. 4b. The result in Fig. 4b enables construction of an empirical relationship approximating the observable shifts:

$$\Delta A \approx \frac{\lambda(s-0.5)^2}{(0.5\pi)^2}, \tag{10}$$

where ΔA is an increment in amplitude caused by the asymmetry of the moiré grating.

Equation 10 is an important approximation for a practicing experimentalist. If the widths of the dark and white bands (in the static moiré grating) are more or less the same, one can relate the order of time-averaged fringe with the magnitude of dynamic deflection (using Eq. 3) with high confidence. If the widths of the dark and white bands are considerably different, one should keep in mind that the centerlines of time-averaged fringes are a little bit shifted compared to the classical result in Eq. 3. However, this shift is rather small. Moreover, it is not so easy to determine the exact centerline by a naked eye (Fig. 3a and b). Thus, the magnitude of the shift of the centerlines should fall into the general budget of uncertainties if the detection of the time-averaged fringes is performed without digital image processing techniques. We demonstrate the fact by an experimental test setup comprising a rubber sample, shaker, and a digital camera (Fig. 5).

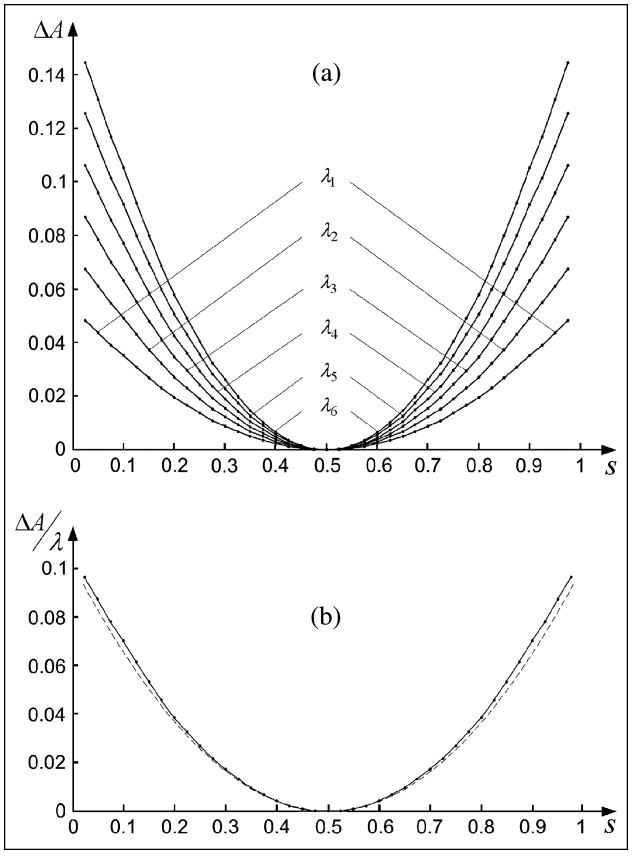

Fig. 4: Shifts of the centerlines of time-averaged fringes: (a) shifts at different pitches: $\lambda_1 = 1.5$, $\lambda_2 = 1.3$, $\lambda_3 = 1.1$, $\lambda_4 = 0.9$, $\lambda_5 = 0.7$, $\lambda_6 = 0.5$ and (b) nondimensional shifts; solid line represents numerically measured shifts and dashed line represents analytical approximation

EXPERIMENTAL INVESTIGATIONS

First, an array of dark bands is formed on the flat surface of a rubber bar. The pitch of the grating is $\lambda = 1$ mm; the width of dark and white bands coincide ($s = 0.5$). The left part of the rubber bar is fixed to a shaker. The frequency of the shaker is set to a level, which corresponds to the second natural frequency of the rubber bar: $\omega = 25$ Hz (Fig. 6a). The pattern of time-averaged fringes is visible by a naked eye—it is also well identifiable in an image produced by digital camera with exposure time $T = 2s$.

Next, the moiré grating (the array of dark bands) is washed from the surface of the rubber bar, and another asymmetric moiré grating is formed on the same surface. The pitch of the grating is kept the same; the coefficient of asymmetry is $s = 0.75$. The rubber bar is again fixed at the same position, and the frequency is again set to $\omega = 25$ Hz which guarantees the same field of dynamic deflections as in the previous experiment (Fig. 6b).

The patterns of time-averaged fringes in Fig. 6a and b look very much alike. As mentioned previously, it is quite hard to detect the exact location of the centerline of a time-averaged fringe by a naked eye. Of course, digital image processing techniques could detect the shift of the centerlines of fringes generated by the asymmetric grating.

In fact, one can construct even more complex gratings than stepped grayscale functions. We still consider an array of parallel bands, but we assume that the variation of the grayscale level in a band can be much more complex than a stepped function. As an example, we generate a set of random numbers evenly distributed in interval [0;1] and interpolate these numbers in one pitch of the grating (Fig. 1c). Computational experiments (Fig. 7) show that even stochastic (but necessarily periodic) moiré grating can produce interpretable time-averaged fringes. If the main peak of the Fourier amplitude spectrum of the stochastic signal determining grayscale

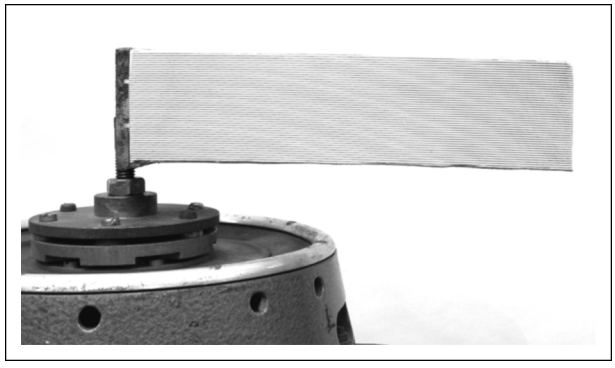

Fig. 5: Experimental setup comprising shaker and rubber bar with moiré grating printed on its surface

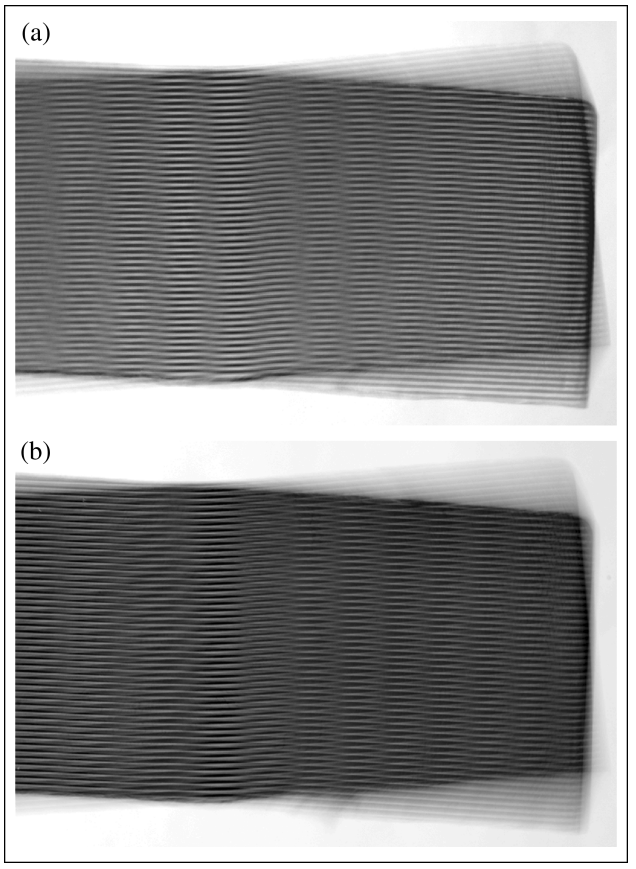

Fig. 6: Experimental time-averaged images: (a) symmetric grating, $s = 0.5$ and (b) asymmetric grating, $s = 0.75$

variation inside one pitch occurs at frequency $\frac{2\pi}{\lambda}$ (Fig. 1c), one can be more or less sure that time-averaged fringes indicate dynamic displacements within the limits of engineering accuracy, though it could be quite hard to detect the centerlines of time-averaged fringes by a naked eye (Fig. 7). Anyway, one must be very careful with the interpretation of time-averaged digital image if the peaks of other frequencies in the Fourier

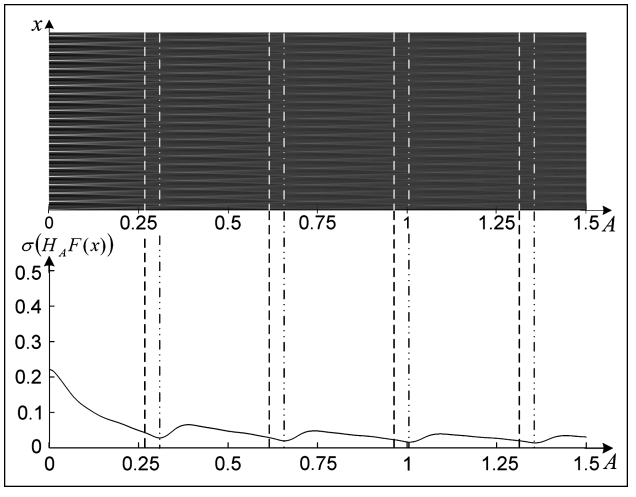

Fig. 7: Computationally reconstructed pattern of fringes for stochastic grayscale moiré grating

amplitude spectrum would be comparable to the main peak corresponding to the dimension of the pitch of the grating.

CONCLUSIONS

The objective of this article was to demonstrate the effects of the structure of moiré gratings to time-averaged moiré fringes. It must be noted that only gratings comprised from arrays of parallel lines are considered here. Nevertheless, the apparent simplicity of the problem is misleading—explicit relationship among the fringe order, pitch of the grating, and dynamic displacement is available only for grayscale harmonic gratings. It is clear that it is unrealistic to expect that a practicing experimentalist would contemplate a grating with harmonic variation of grayscale level—instead, one would use a simple array of dark and white lines.

It is shown that the centerlines of time-averaged fringes produced by stepped symmetric and harmonic moiré gratings coincide (as expected). But the situation becomes more complex when the widths of dark and white bands (in a pitch of the grating) are not equal. Then, the centerlines of time-averaged fringes are shifted in the amplitude domain. Surprisingly, these shifts occur in the same direction, whether the width of the dark band is larger or smaller than the width of the white band.

Advanced strain measurement and control tools (including geometric moiré techniques) are regarded as primary technology drivers in such industries as micro-electro-mechanical systems fabrication and high-precision machine tools manufacturing. Accurate interpretation of experimental measurement results is one of the crucial factors enabling minimization of the general uncertainty budget. Therefore, one must pay considerable attention to the formation of moiré gratings before straightforward interpretation of the experimental results.

References

1. Kobayashi, A.S. *Handbook on Experimental Mechanics*, 2nd Edition, SEM, Bethel, CT (1993).

2. Patorski, K., and Kujawinska, M., *Handbook of the Moiré Fringe Technique*, Elsevier, Amsterdam (1993).

3. Field, J.E., Walley, S.M., Proud, W.G., Goldrein, H.T., and Siviour, C.R., "Review of Experimental Techniques for High Rate Deformation and Shock Studies," *International Journal Impact Engineering*, **30**(7): 725–775 (2004).

4. Post, D., Han, B., and Ifju, P., *High Sensitivity Moiré: experimental Analysis for Mechanics and Materials*, Springer Verlag, Berlin (1997).

5. Dai, F.L., and Wang, Z.Y., "Geometric Micron Moiré," *Optics and Lasers in Engineering* **31**(3): 191–198 (1999).

6. Liang, C.Y., Hung, Y.Y., Durelli, A.J., and Hovanesian, J.D., "Time-Averaged Moiré Method for In-Plane Vibration Analysis," *Journal Sound and Vibration* **62**(2): 267–275 (1979).

7. Ragulskis, M., Ragulskis, L., and Maskeliunas, R., "Applicability of Time Average Geometric Moire for Vibrating Elastic Structures," *Experimental Techniques* **28**(4): 27–30 (2004).

8. Ragulskis, M., and Navickas, Z., "Hash Function Construction Based on Time Average Moiré," *Discrete and Continuous Dynamical Systems-Series B* **8**(4): 1007–1020 (2007).

9. Ragulskis, M., and Navickas, Z., "Representation of Time Averaged Vibrating Images in the Operator Format," *Journal of Vibroengineering* **9**(4): 1–8 (2007). ■